PROCEEDINGS A

rspa.royalsocietypublishing.org

Research

Cite this article: Watanabe Y, Ingram DM. 2016 Size distributions of sprays produced by violent wave impacts on vertical sea walls. *Proc. R. Soc. A* **472**: 20160423. http://dx.doi.org/10.1098/rspa.2016.0423

Received: 30 May 2016
Accepted: 12 September 2016

Subject Areas:
fluid mechanics, wave motion, ocean engineering

Keywords:
flip-through, wave impact, sea spray, spray size distribution, droplet number density

Author for correspondence:
Y. Watanabe
e-mail: yasunori@eng.hokudai.ac.jp

Size distributions of sprays produced by violent wave impacts on vertical sea walls

Y. Watanabe[1] and D. M. Ingram[2]

[1]Graduate School of Engineering, Hokkaido University, North 13 West 8, Sapporo, Japan
[2]School of Engineering, University of Edinburgh, Edinburgh EH9 3JL, UK

YW, 0000-0001-8338-8271

When a steep, breaking wave hits a vertical sea wall in shallow water, a flip-through event may occur, leading to the formation of an up-rushing planar jet. During such an event, a jet of water is ejected at a speed many times larger than the approaching wave's celerity. As the jet rises, the bounded fluid sheet ruptures to form vertical ligaments which subsequently break up to form droplets, creating a polydisperse spray. Experiments in the University of Hokkaido's 24 m flume measured the resulting droplet sizes using image analysis of high-speed video. Consideration of the mechanisms forming spray droplets shows that the number density of droplet sizes is directly proportional to a power p of the droplet radius: where $p = -5/2$ during the early break-up stage and $p = -2$ for the fully fragmented state. This was confirmed by experimental observations. Here, we show that the recorded droplet number density follows the lognormal probability distribution with parameters related to the elapsed time since the initial wave impact. This statistical model of polydisperse spray may provide a basis for modelling droplet advection during wave overtopping events, allowing atmospheric processes leading to enhanced fluxes of mass, moisture, heat and momentum in the spray-mediated marine boundary layer over coasts to be described.

1. Introduction

Sea sprays have important roles for meteorological and environmental processes; examples include the exchanges of gases, moisture and heat, transport of chemical materials [1] and the dynamics of the

THE ROYAL SOCIETY PUBLISHING

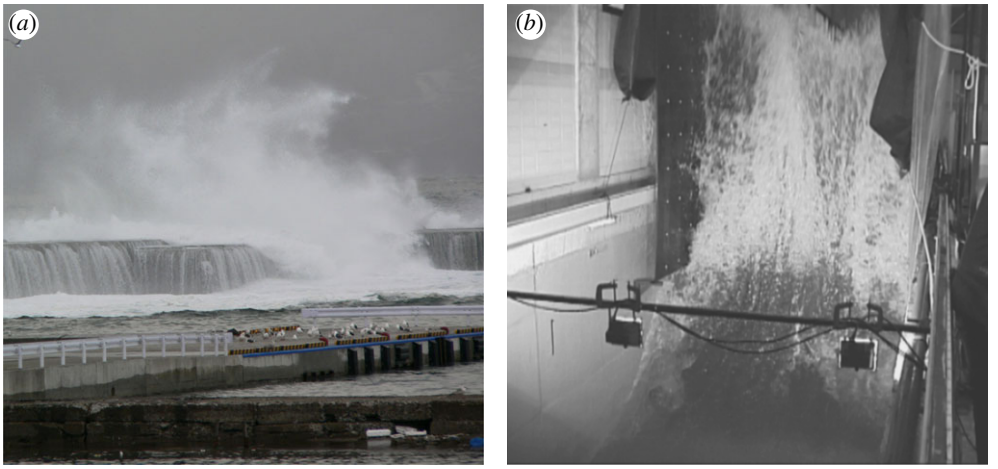

Figure 1. Sea spray created by the impact of large breaking waves on the breakwater at Iwanai Port, Japan (*a*), and a violent wave impact on a 10 : 1 battered wall in the large wave flume at UPC, Barcelona, Spain (*b*; after [11]). (Online version in colour.)

marine atmospheric boundary layer [2]. The contributions of sea sprays to particular atmospheric processes depend on the size distributions of the spray. This in turn defines the total surface area, where mass exchanges occur via dissolution and evaporation, and the concentration and residence time in the atmosphere, which modify momentum transport between air and water as additional drag forces. In the surf zone, there is a variety of size ranges of the spray, each determined by the multitude of primary spray production mechanisms. These range from the finest (sea spray aerosol) created by bubble-bursting at the sea surface [3], through larger spume droplets created by the tearing of wave crests by the wind [4,5], to the largest droplets that are fragmented from finger jets formed by vorticity instability in plunging waves [6,7]. Furthermore, during storm events, when large ocean waves impact on breakwaters and coastal cliffs, sea sprays rising several tens of metres into the air have often been observed in coasts (figure 1*a*). In this case, further downwind transport of the sea sprays and longer residence time, depending on the size distributions, from higher source levels may largely affect the atmospheric dynamics in a thicker spray-mediated boundary layer. However, the spray size distribution associated with violent wave overtopping events has not yet been identified.

The free-surface dynamics of overtopping water waves was discussed in Watanabe & Ingram [8] and may be summarized as follows: when a shoaling wave crest approaches a vertical wall, the wall prevents the forward flow of water, causing the water level at the wall to rise rapidly. The water surface between the rising wave trough and advancing crest converges rapidly, resulting in the violent ejection of a sheet, the so-called flip-through event [9,10]. Large- and small-scale experiments [11] and computer simulations [12] have shown that the velocity of the up-rushing jet can be 8–10 times the inshore wave celerity. As the sheet of water rises, it evolves cusp-like formations which are amplified to produce finger jets and ligaments subsequently fragmented into droplets (figure 1*b*). The instability modes and mechanical processes causing this fragmentation have been described previously [8]. This paper focuses on the question of which probability density function (PDF) best describes the spray droplet distribution in the polydisperse spray during this violent wave overtopping event.

Polydisperse sprays occur in many engineering applications, including fuel injection, agricultural irrigation, the application of pesticides and herbicides, painting and coating surfaces, spray drying, etc. One approach to modelling the spray is to use a PDF to represent the probable number of droplets with certain diameters and velocities in a given region [13–17]. The Rosin–Rammler distribution was suggested [18] and has been found to be appropriate for many types of atomization spray [19]. However, Eggers & Villermaux [20] and Villermaux *et al.* [21] suggested

that the Γ distribution is more appropriate for cases where droplets are torn from fluid ligaments in a gas stream. In cases where there are multiple droplet collisions the lognormal distribution has been suggested [22,23] to be appropriate. The lognormal distribution applies in situations where the interactions of positive random variables are multiplicative rather than additive. Recent work has shown that the lognormal can also apply to additive, positive, random scalar fields such as those found in turbulence [24].

While the Rossin–Rammler, Γ and lognormal PDFs have all been proposed as models of spray sizes in polydisperse sprays the formation mechanisms for the polydisperse sprays are different from those in the present case. Watanabe & Ingram [8] found that two distinct mechanisms govern the break-up of the rapidly ascending liquid sheet formed during a flip-through event: initial amplification of undulations in the sheet thickness resulting in the formation of ligaments which fragment into droplets; and transverse deformations of the rim bounding the liquid sheet form finger jets which, due to capillary instability, also break up to form droplets. The reader is referred to the video in the electronic supplementary material accompanying [8], which shows the break-up of the liquid sheet following a flip-through event. In this paper, the kinematic and geometric features of droplets formed by the fragmentation of the unstable rim–sheet system are discussed and an appropriate PDF is identified to describe the polydisperse spray formed by the wave impact. The results presented here continue the analysis presented in [8] and are based on the same set of experiments. Here, we consider the resulting spray, where Watanabe & Ingram [8] describe the break-up of the up-rushing sheet–rim system.

The paper is organized as follows. In §2, the experimental set-up and conditions are explained. Section 3 discusses the kinematic and geometric features of the droplets fragmented from the unstable rim and sheet system observed experimentally following the wave impact. The PDF describing the droplet size distribution is identified. Finally, the results are summarized in §4.

2. Experiments

This section briefly explains the fundamental experimental methods and conditions used to study the flip-through events. The experimental set-up is described in detail in [8], to which the reader is referred for more detail.

The experiments were conducted in the 24 m long wave flume at the University of Hokkaido, Japan. The 0.6 m wide, 1 m deep flume is fitted with a piston-type wave maker with active wave absorption. A transparent acrylic rectangular box, 0.2 m long and 0.6 m wide with a height of 1 m, was installed on the 1/20 slope beach to form a breakwater with a vertical seaward face (figure 2). The model breakwater was weighted and anchored to the beach to achieve a stationary wall.

The water in the flume was coloured using the fluorescence dye uranine (sodium fluorescein) to enhance contrast of the liquid region. Uranine excites with blue light (absorbance wavelength of 436 nm) and fluoresces with green light (wavelength of 530 nm). A rectangular blue light-emitting-diode (LED) panel (200 × 100 mm) was set on the back of the transparent front wall of the model breakwater and used to illuminate the dyed water passing over it. An 8-bit high-speed video camera recorded the illuminated area using a 45° angled reflector (figure 2). A low-pass optical filter (less than or equal to 450 nm) was fitted to the camera to eliminate the fluorescent emissions from the liquid and allow only the blue component, from the back light, to be recorded. The concentration of the dye, $0.11\,\mathrm{mg\,l^{-1}}$, was chosen to ensure that there would be no light transmission across a 0.25 mm thick fluid film. The 8-bit 1280 × 1024 pixel images were recorded at 500 Hz with an exposure time of 0.125 ms and were stored on a PC connected to the camera as uncompressed bitmaps. We define the coordinate system for the experiment with the origin at the point of wave breaking in the horizontal shoreward x-axis, the nearside of the flume in the transverse y-axis and at the still water level in the vertical z-axis. The still water depth at the origin $x = 0$ was 100 mm. Throughout the experiments, monochromatic waves with an incident wave height of 146 mm and a wave period of 1.9 s were used.

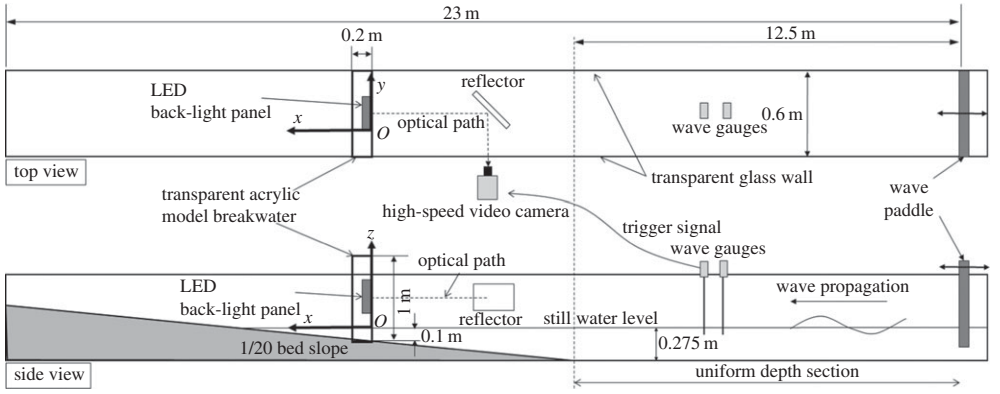

Figure 2. Experimental set-up.

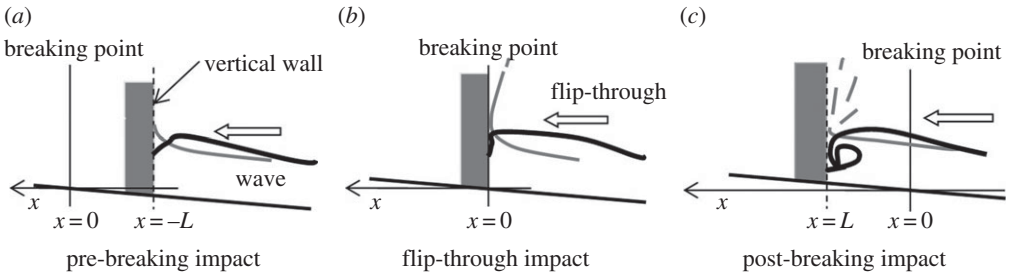

Figure 3. Schematic illustrations of wave impact modes.

The resulting wave impact pressure is very sensitive to the incident wave shape at the impact [25], and consequently the surface behaviour of the vertical jets also depends strongly on the surface shape of the wave face (or local wave steepness). In general, progressive waves with mild steepness reflect off the wall and behave like standing waves at the wall, while steeper waves produce more violent impacts, causing highly accelerated thin up-rushing fluid jets (figure 3). The post-breaking-wave impact provides more complex fluid flows involving entrained air bubbles and induced turbulence. During the experiments, the model breakwater was located at $x = -300, -200, -100$ mm (in the pre-breaking region), 0 mm (for the flip-through mode) and 200 mm (for the post-breaking region). The region illuminated by the LED panel was also traversed vertically from 50 mm above the still water level to +800 mm at 50 mm intervals to allow the vertical evolution of the jets to be examined. The 20 trials of the experiments were performed at each level to allow a statistical analysis of the results.

Noise on the acquired images was reduced using a median filtering operation. Image coordinates were transformed to real coordinates using a linear image transformation, providing quantitative measures of the liquid surface on images at 0.10 mm pixel^{-1} resolution.

Each frame from the video was post processed using the energy-fitting algorithm level-set method [26]. This allows the detection of both the boundaries of the liquid jet and the individual spray droplets. In the present results, droplets are defined as regions having a closed boundary while the jet boundary must intersect the edge of the image (figure 4). Liquid, which is out of the focal plane of the camera and which has the maximum absolute gradient of image intensity along the liquid boundaries lower than a given threshold, is removed from ensemble statistics. This approach allows us to distinguish between the liquid jet and the spray droplets and, in this paper, concentrate our attention on the spray.

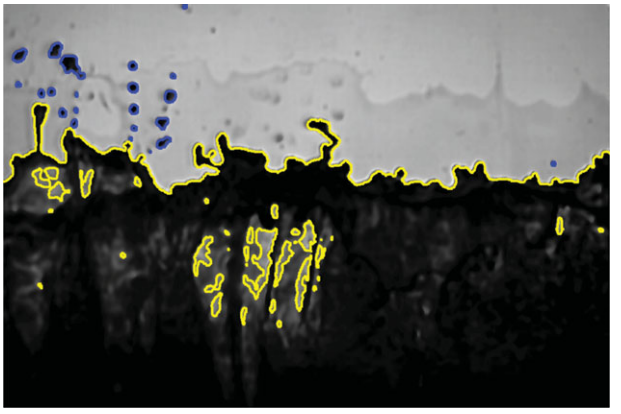

Figure 4. The detected interface boundary for the typical back-light images of the jets (yellow line) and dispersed sprays (blue line).

3. Results

The features of the ascending planar jet and those of the resulting spray population depend strongly on the relative position of the vertical sea wall to the point at which the wave breaks. As the jet rises, undulations in the thickness of the fluid sheet are rapidly amplified and ruptured into an array of vertical ligaments, while lateral undulations of the rim lead to the formation of finger jets that subsequently break up to form droplets and spray. The underlying processes are described in detail in [8]. In this section, we describe the impact of wall location on the spray velocity and droplet population. A consideration of the processes leading to droplet formation are then described, characterizing the spray size distributions observed following a flip-through event. Finally several of the PDFs suggested as descriptions of polydisperse sprays are considered and an appropriate model identified.

(a) Spray velocity and population

The spray formation depends strongly on whether the sea wall is impacted by a pre-breaking, breaking or broken wave. No spray was observed in the wall location $x < -100$ mm. In this region, a vertical planar sheet is stretched from the crest of a standing wave as it runs up on the wall (see figure 3*a*; also see fig. 8 *a*,*b* in Watanabe & Ingram [8]). In shallower locations, the spray population increases with relative wall distance x (figure 5*a*), as the rim and sheet of the ascending jet successively break up into droplets. In the flip-through case ($x = 0$), the initial high acceleration of the jets enhances both sheet stretch and the unstable surface behaviours, resulting in a large number of spray droplets ascending at higher velocity (figure 5*b*). A parabolic increase in the spray population with vertical measurement level is observed in this case (figure 5*a*). The maximum population of spray droplets is achieved in the post-breaking case ($x = 200$ mm), where complex shaped jets are initially blown out by the collapse of an air pocket squeezed between the overturning jet and the sea wall, and the additional spray production is enhanced through the bubble-bursting. In all cases where sea sprays are formed, the fragmented spray rises much faster than the jet at each measurement level (figure 5*b*); an analysis of the video images shows that this is in the region of 1.3–1.5 times faster for $x = -100$ and 0 mm and between 1.6 and 2.7 times faster for $x = 200$ mm.

While a study of the post-breaking spray, where the maximum population is achieved, would be interesting, the mechanical parameters affecting the break-up of the jet, beyond capillary dynamics, are unknown. Since the post-breaking waves entrap an air pocket and entrain air bubbles before the impact [6,25], the bubble-bursting may become an additional mechanism

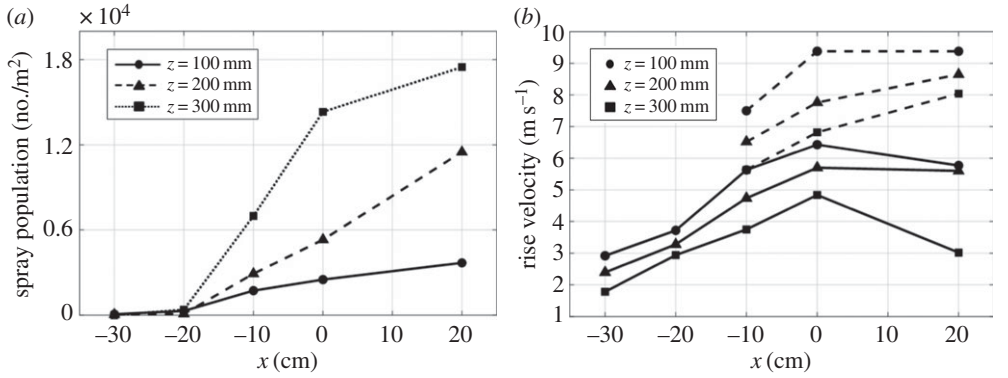

Figure 5. Spray population (*a*) and the ensemble mean rise velocities of the ascending jets (solid line) and sprays (broken line) (*b*) with respect to the relative wall distance from the breaking location.

for the spray production, which is beyond the scope of this study. We have therefore left this case for future investigation and will focus on the flip-through case to identify the statistical features of the spray break-up resulting from consecutive unstable surface deformation described by Watanabe & Ingram [8].

(b) Spray size

In this section, we discuss the break-up mechanisms of the flip-through jets during the unstable deformation of the rim–sheet system.

At the beginning of a flip-through event, as the sheet is ejected, a rim is formed at the leading edge of the jet (figure 6*a*). This rim deforms transversally, forming finger jets during the retraction process when the sheet is vertically stretched beneath the rim. Transverse undulations in sheet thickness are amplified, causing the sheet to rupture (figure 6*c*). As the holes in the sheet extend, multiple vertical ligaments connected to the deformed rim form a rim–ligament system of jets (figure 6*e*). Finally, capillary instabilities cause the sequential break-up of the ligaments into droplets. This process is illustrated in figure 7.

According to Watanabe & Ingram [8], the maximum unstable growth appears in the low-wavenumber range at the early stage of the flip-through event. As the flip-through event develops the unstable dimensionless wavenumber, $\kappa_{max} = k_{max} a_i$, shifts towards a higher wavenumber, approaching 0.7, which corresponds to the Rayleigh–Plateau mechanism. Here, the dimensional wavenumber $k_{max} = 2\pi/l_{max}$ and a_i is the initial rim radius. The most unstable (dimensional) wavelength, l_{max}, which governs the transverse spacings of the ligaments (figure 7*a*), is therefore a function of rim acceleration $\dot{v}_{ri}$. This can be described using the transitional unstable wavenumber $\kappa_{max}(\dot{v}_{ri})$,

$$l_{max} = \frac{2\pi}{\kappa_{max}} a_i. \tag{3.1}$$

The number of ligaments in a transverse length L, n_{lf}, can be written by

$$n_{lf} \sim \frac{L}{l_{max}} \approx L \frac{\kappa}{2\pi} a_i^{-1}. \tag{3.2}$$

It can be assumed that the droplets are successively formed at frequency f_d from a single ligament during the initial ligament break-up (figure 7*b*), following the analogy of the capillary break-up of a cylindrical jet [27]. The transitional number of droplets formed along the ligament, n_d, in the time t elapsed since the start of the break-up is given by

$$n_d \sim f_d t \approx \sigma_{max} t; \tag{3.3}$$

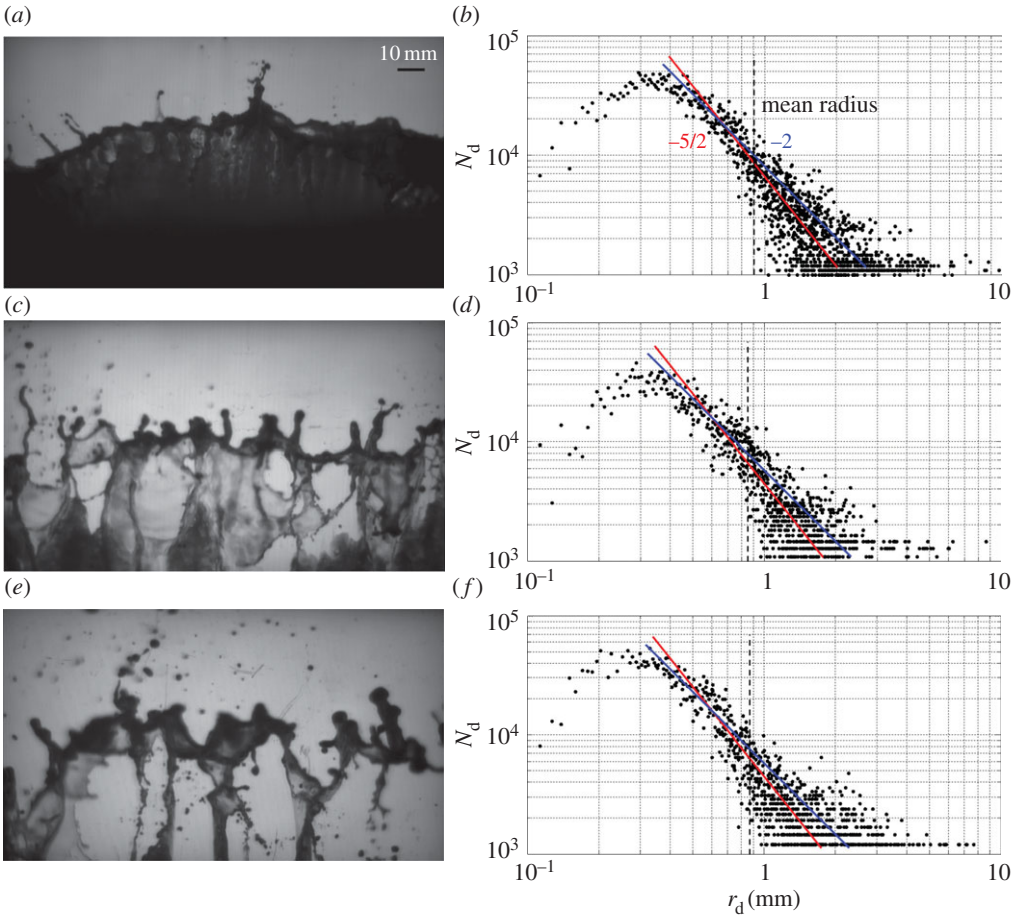

Figure 6. Transverse surface forms of the flip-through jet (*a*,*c*,*e*) and spray size distributions (*b*,*d*,*f*), defined by the number of spray droplets per cubic metre in a bin radius of 1 µm versus spray radius for 20 trials; vertical level $z = 50$ mm (*a*,*b*), $z = 150$ mm (*c*,*d*) and $z = 250$ mm (*e*,*f*). The red and blue lines represent $-\frac{5}{2}$ and -2 slopes, respectively.

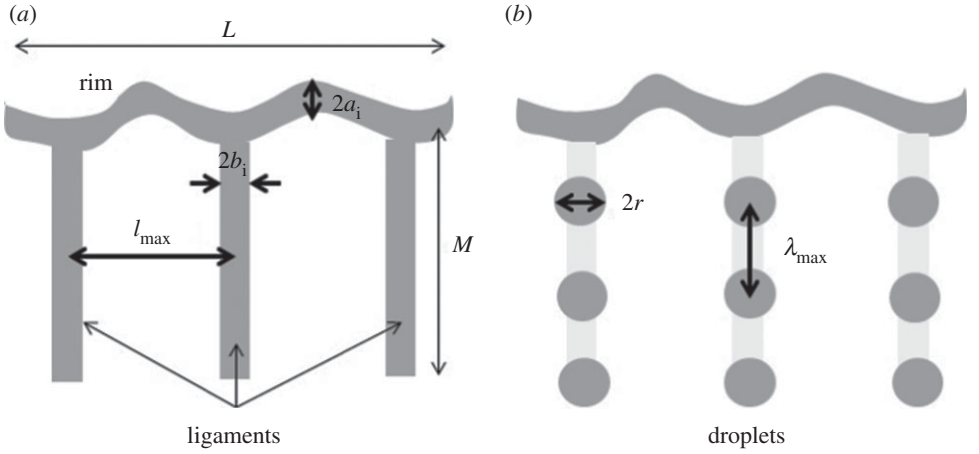

Figure 7. Schematic of the deformation and break-up of the flip-through jets; (*a*) a deformed rim connected to vertical ligaments, resulting from instabilities of the rim–sheet system, and (*b*) break-up of the ligaments owing to capillary instability.

the maximum growth rate σ_{max} for the capillary instability is

$$\sigma_{max} = C_d \left(\frac{\gamma}{\rho b_i^3} \right)^{1/2}, \tag{3.4}$$

where γ, ρ and b_i are the surface tension, liquid density and the initial ligament radius, respectively. For the Rayleigh–Plateau instability on a cylindrical liquid jet, the constant C_d is numerically approximated as $C_d \approx 0.12$ [27].

We can now write the steady-state droplet population, n_{df}, due to break-up at the most unstable (dimensional) wavelength $\lambda_{max} = C_{df} b_i$, with ligament length M in the fully fragmented stage (figure 7*b*), as

$$n_{df} \sim \frac{M}{\lambda_{max}} \approx M C_{df}^{-1} b_i^{-1}, \tag{3.5}$$

where the constant C_{df} for an unstable cylindrical jet is numerically estimated to be 9.02 [27]. Equating this with equation (3.3) temporally integrated from the inception of break-up to the time to achieve the fully fragmented state, we find that the droplet formation occurs in the range $0 \leq t \leq (2M)^{1/2}(C_d C_{df} u_c)^{-1/2}$ of the break-up period, where capillary velocity $u_c = \sqrt{\gamma/\rho b_i}$. Furthermore, the integrated number of droplets formed in the rim–ligament system until t in the early stages of the break-up process, N_e, can be estimated as

$$N_e \sim \frac{n_{lf} n_d t^2}{2} \approx C_e a_i^{-1} b_i^{-3/2} t^2 \approx C_e a_i^{-5/2} t^2, \tag{3.6}$$

assuming identical rim and ligament radii $a_i \approx b_i$, where C_e is the constant. The temporal increase of N_e is consistent with the observed parabolic increase in the spray population with measurement level, shown in figure 5*a*. When the ligaments are fully fragmented into droplets, the total number of droplets formed in the rim–ligament system at the steady state, N_s, may be approximated as

$$N_s \sim n_{lf} n_{df} \approx C_s a_i^{-1} b_i^{-1} \approx C_s a_i^{-2}, \tag{3.7}$$

where C_s is the constant.

Rutland & Jameson [28] used theory to predict the volumes of the main and satellite droplets fragmented from a liquid jet with radius a_i and compared this with measured droplet sizes. They found the theoretical droplet size associated with the most unstable wavenumber, $r = 1.89 a_i$. As the radius r can be assumed to be proportional to a_i for equations (3.6) and (3.7), the total droplet numbers are therefore related to the drop radius

$$N_e \propto r^{-5/2} \tag{3.8}$$

and

$$N_s \propto r^{-2}. \tag{3.9}$$

Figure 6 shows the droplet size distributions plotted on log–log axes as number density, N_d (representing the number of droplets per cubic metre in each 1 µm radius bin), against the equivalent radius of the droplet area detected on the experimental images, r_d, together with the transverse surface forms of the flip-through jet at the corresponding level from $z = 50$ to 250 mm.

While there is active deformation of the unstable surface of the jet at the early stage of the flip-through event, the observed size distributions are similar, in a larger range than the radius with the maximum density, at all three measurement levels with $\ln N_d$ decaying with $\ln r_d$, while the dispersions increase with r_d. The plots show that the number densities in the larger radius range are well approximated by a $-5/2$ slope (denoted by a solid red line) and a -2 slope (a solid blue line)—a result which is consistent with our estimates of the total droplet numbers given by equations (3.8) and (3.9). The observed dispersion may be associated with nonlinear growth of the unstable deformations, formations of the satellite drops [28] and variable ligament sizes, all of which are neglected in our linear stability analysis of the rim–sheet system [8]. There are large changes in the exponential gradient of the experimental droplet sizes in the small size range ($r_d < 0.4$ mm), suggesting that break-up of the small droplets is governed by dynamics, other than

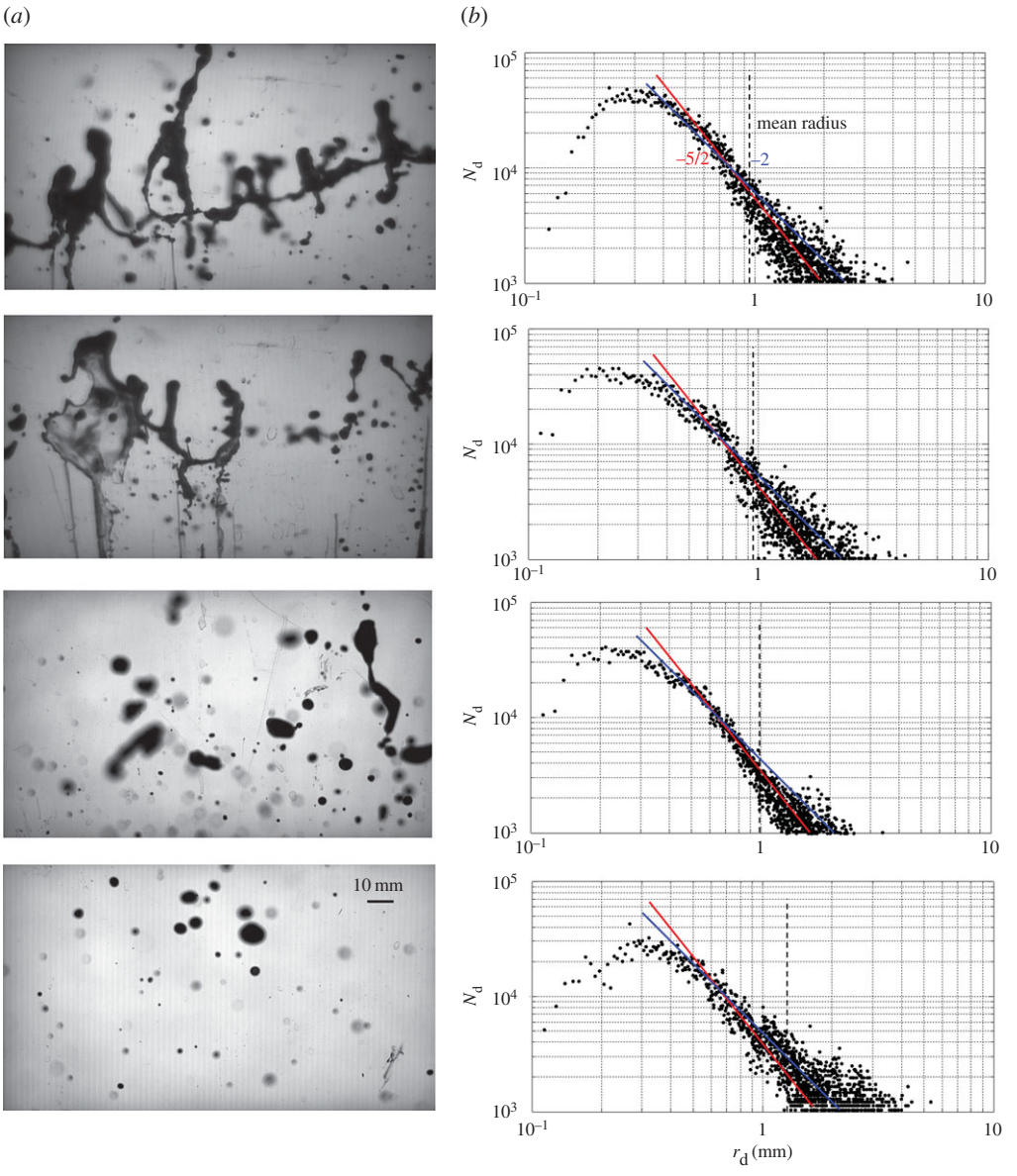

Figure 8. Transverse surface forms of the flip-through jet (*a*) and spray size distributions (*b*), defined by the number of spray droplets per cubic metre in a bin radius of 1 μm versus the spray radius for 20 trials; vertical level $z = 350, 450, 600, 800$ mm from top to bottom. The red and blue lines represent $-5/2$ and -2 slopes, respectively.

those described above, during the sequential break-up process from larger droplets into smaller ones. The formation of smaller droplets is therefore likely to break the assumption made in the current droplet number models. Consequently, the models are only applicable to large droplets ($r_d > 0.4$ mm).

As the rim and sheet continue to disintegrate they are successively fragmented into spray (figure 8). The spray then continues to ascend but no further break-up behaviour is observed. By $z = 800$ mm, it is clear that the break-up process has been terminated before the spray arrives at this level as no ligaments from either the fragmented rim or the sheet are observed. In this fully fragmented state, the steady size distribution (3.9) provides a more appropriate approximation of the observed spray than the transitional model (3.8).

While the larger ranges of the size distribution, which can be approximated by equations (3.8) and (3.9), are unchanged over measurement levels, the droplet radius associated with the maximum number density decreases with level because of successive break-ups below the level $z = 600$ mm. The following droplet radii are observed in the experimental data: 0.29 mm at $z = 200$ mm, 0.27 mm at $z = 400$ mm, and finally 0.20 mm at $z = 600$ mm.

We find a decrease in the population of the small size range at $z = 800$ mm, while the population of larger droplets remains unchanged, resulting in a relative increase in the maximum and mean drop radius from the lower level. Since the drag forces acting on the ascending fragmented droplets are size dependent, they have a variety of rise velocities depending on the local size distribution at this stage. As smaller droplets may be decelerated more than larger ones and fall at lower levels, the relative number of smaller droplets is reduced to be recorded at a high measurement level where new production of small droplets due to break-up has been terminated. Evaporation may also have a small effect on the observed distribution, but this is left for future investigations.

(c) Probability distribution

While the models above apply only to the larger droplet sizes, statistical PDFs can be used to describe the number density distribution over the whole range of droplet sizes. Several different PDFs have been suggested.

Villermaux *et al.* [21] found that the Γ distribution provides a good model for the PDF of the size of spray droplets fragmented from ligaments torn off from the liquid jet in a gas stream. The same distribution has also been shown to provide a good model for the fragment sizes for liquid sheets resulting from the oblique collision of two cylindrical jets [29] and for an axisymmetric expanding sheet formed by the impact of a steady gravity-driven circular jet and droplet onto the horizontal upper surface of a solid cylinder [30,31]. The Γ distribution is

$$p_\Gamma\left(x = \frac{d}{\bar{d}}\right) = \frac{n^n}{\Gamma(n)} x^{n-1} \exp(-nx), \tag{3.10}$$

where d is the spray diameter and $\bar{d}$ is the mean diameter. A parameter n is chosen to reflect the initial configuration of the ligaments. $n \sim 4$–5 is suggested by Bremond *et al.* [30].

Roisman *et al.* [32] proposed the Weibull distribution as an empirical approximation of the PDF of secondary droplets generated through the rim instability of crown splashes,

$$p_W(x) = \frac{\beta}{\alpha}\left(\frac{x}{\alpha}\right)^{\beta-1} \exp\left(-\left(\frac{x}{\alpha}\right)^{\beta}\right), \tag{3.11}$$

where the parameters α and β are again estimated empirically. Another alternative is the lognormal distribution,

$$p_{\ln}(x) = \frac{1}{x\lambda\sqrt{2\pi}} \exp\left(\frac{-(\ln x - \mu)^2}{2\lambda^2}\right), \tag{3.12}$$

where the logarithmic average μ and standard deviation λ are determined by fitting procedures.

Figure 9 shows the PDFs for the Γ, Weibull and lognormal distributions fitted to the experimental data. The Γ distribution with $n = 2$, $n = 3$ or $n = 5$ provides a poor fit to the data, while the Weibull distribution model performs well for large droplet sizes with $d/\bar{d} > 2$ but performs poorly for smaller droplets. By contrast, the lognormal distribution fits the data well across the whole $d/\bar{d}$ range. The deviation from the Γ and Weibull distributions indicates that the underlying spray formation mechanisms are different from those discussed by [30,32]. There are major differences between the initial unstable behaviours in the flip-through events [8], undulating liquid sheet [30] and crown splashes [32] which lead to different droplet size distributions. The dynamics of the coupled rim–sheet, leading to the transitional rim–ligament system, discussed in §3b, defines the distinct initial conditions for the number density of the droplets fragmented from the system.

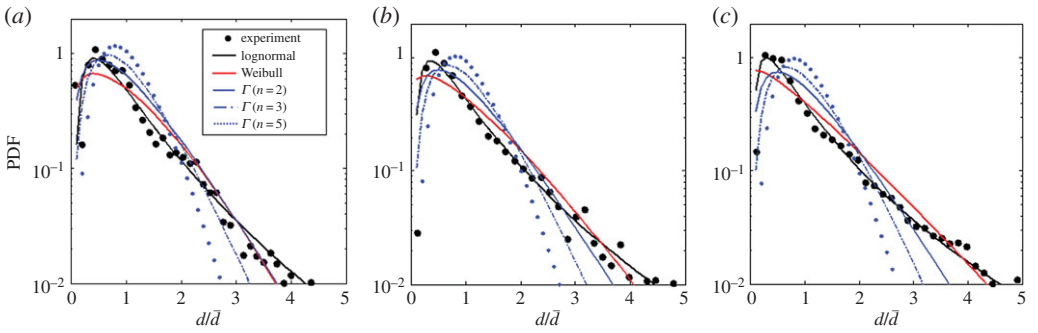

Figure 9. PDFs of the normalized spray size; $z = 200$ mm (*a*), $z = 400$ mm (*b*) and $z = 600$ mm (*c*).

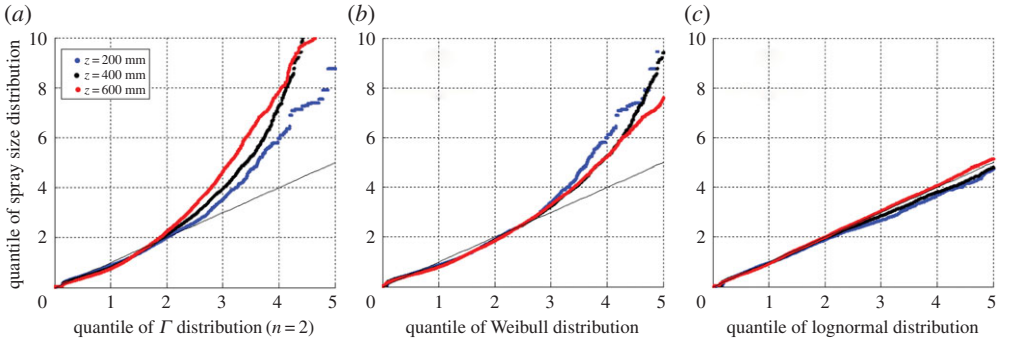

Figure 10. Quantile–quantile plots for the experimental spray size distributions against the $\Gamma(n = 2)$ (*a*), Weibull (*b*) and lognormal (*c*) distributions.

Our initial investigation, of which the three proposed PDFs fit the data, begins by examining quantile–quantile (QQ) plots of the measured and modelled spray size distributions. QQ plots plot the ranked experimental data against the equivalent quantiles of the theoretical distribution. If the distribution provides a good fit for the data the observations will lie on the 45° line. It should be noted that, even in the case of a good fit, the extreme values will often lie off the line. Figure 10 shows QQ plots for the experimental spray size measurements against the $\Gamma(n = 2)$ (figure 10*a*), Weibull (figure 10*b*) and lognormal (figure 10*c*) distributions. The QQ plots for the $\Gamma(n = 2)$ and Weibull distributions clearly show that the quantiles of the distributions do not fit with those of the experimental data. In both values above the medians lie far from the line, indicating a poor fit. The QQ plots provide strong, graphical evidence that neither the $\Gamma(n = 2)$ nor the Weibull distributions provide good models for the PDF of the spray size. The lognormal QQ plot, in contrast, shows good agreement between the model and experimental distributions with very little deviance from the straight line at any of the three elevations. This analysis indicates that the mechanisms for the break-up of the spray proposed by [21,32] are different from those associated with the flip-through case and suggests that the lognormal distribution may provide a good model for the spray size PDF.

Stronger statistical evidence of the goodness of fit is obtained by performing the well-known, non-parametric, Kolmogorov–Smirnov test for the fit of a distribution. The Kolmogorov–Smirnov test assesses the null hypothesis that the specified distribution fits the data against the alternative hypothesis that it does not; if the calculated p-value is smaller than 0.05 then there is significant statistical evidence to reject the hypothesis that the data fit the distribution. The test was performed using the R statistics package [33].

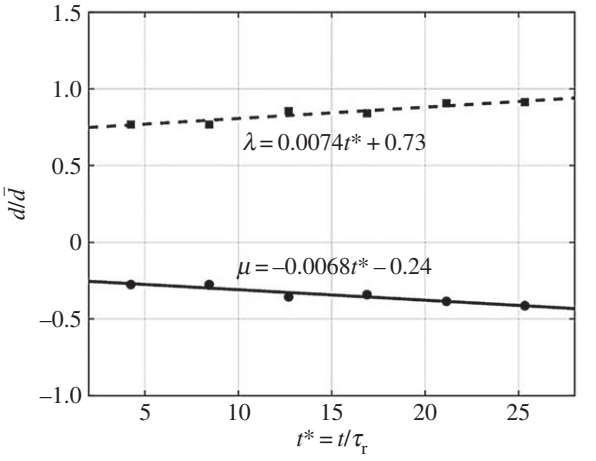

Figure 11. Evolution of the optimal parameters of the lognormal distribution.

The calculated p-values from the tests for fitting the lognormal distribution at the three elevations are: $P_{z=200} = 0.2132$, $P_{z=400} = 0.2649$ and $P_{z=600} = 0.644$. In all three cases, the p-value is greater than 0.05, so we conclude that at the 5% significance level there is insufficient statistical evidence to reject the hypothesis that the lognormal distribution fits the spray size data.

Trietsch & Baker [34] report that while the normal distribution is usually a good representation of the interaction of n, independent, random variables (due to the central limit theorem) it is inadequate for strictly positive variables, since there is a finite probability of having a negative value. They note that in such cases the lognormal distribution may be appropriate. Mouri [24] shows that the lognormal is also a good approximation for small n. Since droplet size must be strictly positive, and in the formation of the spray droplet collisions are likely to occur, it seems likely that the conditions noted by Trietsch & Baker [34] and Mouri [24] are met. The lognormal distribution is widely accepted to describe populations of observed atmospheric aerosol particles, including sea spray aerosol that exhibits multiple lognormal modes [35,36], which provides a consistent analogy with the present analysis, although the size range reported is orders of magnitude smaller than those involved in this study.

In order to provide a general representation of the empirical parameters for the droplet size PDF during the fragmentation process, we introduce the dimensionless time

$$t^* = \frac{t_i}{\tau_r},$$

where t_i is the arrival time of the jet at the vertical level z from the time to start the flip-through and τ_r is the capillary time for the rim deformation, $\tau_r = \sqrt{\rho a_i^3/\gamma}$. The normalized time t^* thus provides a relative measure of the evolution of the capillary deformation. Least-squares estimates for the lognormal parameter μ and λ are shown in figure 11. In all cases linear relationships provide a good fit between the scaled time and the distribution parameters.

The least-squares approximations for the free parameters of the lognormal distribution are

$$\lambda = 0.0074t^* + 0.73 \tag{3.13}$$

and

$$\mu = -0.0068t^* - 0.24, \tag{3.14}$$

indicating that there is a small decrease in the mean droplet diameter with increasing time while the standard deviation increases. The temporal variations of μ and λ interpret the statistical features that the maximum spray number density increases and the prominent spray becomes

finer due to the successive break-up of the rims and ligaments into smaller droplets during the up-rush stage of flip-through jet.

The present analysis provides a physical basis for a statistical model of sea sprays produced by violent wave impacts on sea walls, and other sheer vertical surfaces, along the coastline. The model may lead to further understanding of coastal atmospheric processes occurring at the nexus of the natural and built environment in the marine boundary layer.

4. Conclusion

The fragmentation into spray of the water jet created by flip-through events when a breaking wave impacts on vertical walls has been characterized using image analysis to measure droplet sizes during wave impact experiments and the resulting spray size distributions examined.

A theoretical consideration of the rim–ligament system created by instabilities in the rim–sheet system created by the wave impact [8] shows that for larger droplet sizes the number distribution decays with an exponential $-5/2$ slope for the early transitional stage of the flip-through and -2 slope in the steady, fully fragmented, stage. These estimates are consistent with the experimental data collected.

A comparison of the PDFs proposed for modelling polydisperse sprays (Γ, Weibull and lognormal) shows that the lognormal distribution provides a good statistical fit for sprays resulting from flip-through events. The deviation from the Γ and Weibull distributions is due to different underlying spray formation mechanisms from those for crown splashes and undulating liquid sheets for which the first two distributions are proposed.

Furthermore, linear fits for the mean and standard deviation of the lognormal distribution as functions of rise time have been produced. These fits provide a statistical model that gives a good description of the spray size distribution resulting from a flip-though event.

Coastal sea sprays affect both the dynamics within the marine boundary layer and the downwind environment. Sea sprays produced by violent wave impacts on sea walls, especially during storm events, may rise high into the air, resulting in significant downwind transport of the spray aerosols and high residence times. Such high spray concentrations and long residence times may modify the dynamics of the atmospheric boundary layer. The present statistical model may provide useful, physically rational, descriptions of spray aerosols along the coast, caused by wave impacts on both man-made structures and vertical sea cliffs, leading to improved understanding of coastal atmospheric processes and sea spray transport.

Data accessibility. This article is supported by the identical experimental image data used in [8], including the electronic supplementary material video file of the original image data (movie S1) at http://rspa.royalsocietypublishing.org/content/471/2182/20150397.figures-only.

Authors' contributions. Y.W. and D.M.I. conceived of the research, carried out the analyses, drafted the manuscript and approved the study for publication.

Competing interests. The authors declare that no competing interests exist.

Funding. This research was supported by JSPS Grant-in-Aid for Scientific Research (15H04043).

Acknowledgements. The authors thank S. Ishizaki for his help in conducting experiments.

References

1. O'Dowd CD, Leeuw G. 2007 Marine aerosol production: a review of the current knowledge. *Phil. Trans. R. Soc. A* **365**, 1753–1774. (doi:10.1098/rsta.2007.2043)
2. Kudryavtsev VN, Makin VK. 2011 Impact of ocean spray on the dynamics of the marine atmospheric boundary layer. *Boundary Layer Meteorol.* **140**, 383–410. (doi:10.1007/s10546-011-9624-2)
3. Leeuw G, Neele FP, Hill M, Smith MH. 2000 Production of sea spray aerosol in the surf zone. *J. Geophys. Res.* **105**, 29 397–29 409. (doi:10.1029/2000JD900549)
4. Anguelova M, Barber Jr RP, Wu J. 1999 Spume drops produced by the wind tearing of wave crests. *J. Phys. Oceanogr.* **29**, 1156–1164. (doi:10.1175/1520-0485(1999)029<1156:SDPBTW>2.0.CO;2)

5. Veron F, Hopkins C, Harrison EL, Mueller JA. 2012 Sea spray spume droplet production in high wind speeds. *Geophys. Res. Lett.* **39**, L16602. (doi:10.1029/2012GL052603)
6. Watanabe Y, Saeki H, Hosking RJ. 2005 Three-dimensional vortex structures under breaking waves. *J. Fluid Mech.* **545**, 291–328. (doi:10.1017/S0022112005006774)
7. Saruwatari A, Watanabe Y, Ingram DM. 2009 Scarifying and fingering surfaces of plunging jets. *Coast. Eng.* **56**, 1109–1122. (doi:10.1016/j.coastaleng.2009.08.007)
8. Watanabe Y, Ingram DM. 2015 Transverse deformation of up-rushing jets formed during wave impacts on vertical walls. *Proc. R. Soc. A* **471**, 20150397. (doi:10.1098/rspa.2015.0397)
9. Cooker MJ, Peregrine DH. 1990 A model for breaking wave impact pressure. In *Proc. 22nd Int. Conf. on Coastal Engineering, Delft, The Netherlands, 2–6 July 1990*, pp. 1473–1486. New York, NY: American Society of Civil Engineers.
10. Cooker MJ, Peregrine DH. 1995 Pressure-impulse theory for liquid impact problems. *J. Fluid Mech.* **297**, 193–214. (doi:10.1017/S0022112095003053)
11. Bruce T, Pearson J, Allsop NWH. 2003 Hazards at coast and harbour seawalls—velocities and trajectories of violent ovetopping jets. In *Coastal engineering 2002: solving coastal conundrums*, vol. 2 (ed. J McKee Smith), pp. 2216–2226. Singapore: World Scientific.
12. Ingram DM, Causon DM, Bruce T, Pearson J, Gao F, Mingham CG. 2005 Numerical and experimental predictions of overtopping volumes for violent overtopping events. In *Proc. Coastal Structures 2003, Portland, OR, 25–31 August, 2003*, pp. 631–642. New York, NY: American Society of Civil Engineers.
13. Lasheras JC, Hopfinger EJ. 2000 Liquid jet instability and atomization in a coaxial gas stream. *Annu. Rev. Fluid Mech.* **32**, 275–308. (doi:10.1146/annurev.fluid.32.1.275)
14. Varga CM, Lasheras JC, Hopfinger EJ. 2003 Initial breakup of a small-diameter liquid jet by a high-speed gas stream. *J. Fluid Mech.* **497**, 405–434. (doi:10.1017/S0022112003006724)
15. Gorokhovski M, Jouanguy J, Chtab-Desportes A. 2009 Stochastic model of the near-to-injector spray formation assisted by a high-speed coaxial gas jet. *Fluid Dyn. Res.* **41**, 15. (doi:10.1088/0169-5983/41/3/035509)
16. Gorokhovski M, Herrmann M. 2008 Modelling primary atomization. *Annu. Rev. Fluid Mech.* **40**, 343–366. (doi:10.1146/annurev.fluid.40.111406.102200)
17. Vinkovic I, Aguirre C, Simoëns S, Gorokhovski M. 2006 Large eddy simulation of droplet dispersion from inhomogeneous turbulent wall flow. *Int. J. Multiphase Flow* **32**, 344–464. (doi:10.1016/j.ijmultiphaseflow.2005.10.005)
18. Williams FA. 1961 Progress in spray-combustion analysis. *Symposium* (*International*) *on Combustion* **8**, 50–69. (doi:10.1016/S0082-0784(06)80487-X)
19. Beck JC, Watkins AP. 2003 On the development of a spray model based on drop-size moments. *Proc. R. Soc. Lond. A* **459**, 1365–1394. (doi:10.1098/rspa.2002.1052)
20. Eggers J, Villermaux E. 2008 Physics of liquid jets. *Rep. Progress Phys.* **71**, 79. (doi:10.1088/0034-4885/71/3/036601)
21. Villermaux E, Marmottant P, Duplat J. 2004 Ligament-mediated spray formation. *Phys. Rev. Lett.* **92**, 074501. (doi:10.1103/PhysRevLett.92.074501)
22. Efendiev Y. 2004 Modeling and simulation of multi-component aerosol dynamics. *Comput. Appl. Math.* **23**, 401–423. (doi:10.1590/S0101-82052004000200016)
23. Foissac A, Malet J, Mimouni S, Ruyer P, Feuillebois F, Simonin O. 2013 Eulerian simulation of interacting PWR sprays including droplet collisions. *Nuclear Technol.* **181**, 133–143.
24. Mouri H. 2013 Log-normal distribution from a process that is not multiplicative but is additive. *Phys. Rev. E* **88**, 042124. (doi:10.1103/PhysRevE.88.042124)
25. Peregrine DH. 2003 Water-wave impact on walls. *Annu. Rev. Fluid Mech.* **35**, 23–43. (doi:10.1146/annurev.fluid.35.101101.161153)
26. Chan TF, Vese LA. 2001 An active contour model without edges. *IEEE Trans. Image Process.* **10**, 266–277. (doi:10.1109/83.902291)
27. Levich VG. 1962 *Physicochemical hydrodynamics*, p. 700. Englewood Cliffs, NJ: Prentice-Hall Inc.
28. Rutland DF, Jameson GJ. 1970 Theoretical prediction of the sizes of drops formed in the breakup of capillary jets. *Chem. Eng. Sci.* **25**, 1689–1698. (doi:10.1016/0009-2509(70)80060-4)
29. Bremond N, Villermaux E. 2006 Atomization by jet impact. *J. Fluid Mech.* **549**, 273–306. (doi:10.1017/S0022112005007962)
30. Bremond N, Clanet C, Villermaux E. 2007 Atomisation of undulating liquid sheets. *J. Fluid Mech.* **585**, 421–456. (doi:10.1017/S0022112007006775)

31. Villermaux E, Boosa B. 2011 Drop fragmentation on impact. *J. Fluid Mech.* **668**, 412–435. (doi:10.1017/S002211201000474X)
32. Roisman IV, Horvat K, Tropea C. 2006 Spray impact: rim traverse instability initiating fingering and splash. *Phys. Fluids* **18**, 102104. (doi:10.1063/1.2364187)
33. R Core Team. 2014 *R: a language and environment for statistical computing*. Vienna, Austria: R Foundation for Statistical Computing.
34. Trietsch D, Baker KR. 2012 PERT 21: fitting PERT/CPM for use in the 21st century. *Int. J. Project Manag.* **30**, 490–502. (doi:10.1016/j.ijproman.2011.09.004)
35. Whitby KT. 1978 The physical characteristics of sulfur aerosols. *Atmos. Environ.* **12**, 135–159. (doi:10.1016/0004-6981(78)90196-8)
36. Lewis ER, Schwartz SE. 2004 *Sea salt aerosol production*. Washington, DC: American Geophysical Union.